doi.org/10.1002/batt.202000229
Chem Europ
European C
Societies P
Check for updates

Special Collection

Ionic Conductivity of $Na_3V_2P_3O_{12}$ as a Function of Electrochemical Potential and its Impact on Battery Performance

Tu Lan,*[a, b, c] Qianli Ma,[a] Chih-Long Tsai,[a, d] Frank Tietz,[a] and Olivier Guillon[a, b, c]

$Na_3V_2(PO_4)_3$ (NVP) is a promising electrode material for sodium-ion batteries. However, many of its electrochemical properties like ionic conductivities have never been systematically studied. In the present paper, a battery cell with controlled morphology of NVP was prepared and the electrochemical impedance spectra were measured at various voltages. The ionic conductivity of NVP was calculated in dependence on applied potentials. NVP has a total conductivity of 1×10^{-6} S cm^{-1} at 2.9 V, which decreases to 8×10^{-8} S cm^{-1} at 3.5 V. This low conductivity, especially at higher voltages, influences the performance of batteries with an NVP electrode, especially by limiting the high-rate cycling of solid-state batteries.

1. Introduction

Sodium-ion batteries (NIBs) have received increasing research interest as an economic and ecological alternative to the widely used Li-ion batteries.[1] For NIBs, $Na_3V_2(PO_4)_3$ (NVP) is a promising electrode material, which crystallizes in the NaSICON (Na Super-Ionic CONductor) structure (kosnarite-type structure).[2] NVP was first reported by Delmas et al. in 1978 after the crucial discovery of NaSICON materials by Hong and Goodenough.[3] Afterwards, several reports were published on its structure[4] and on its potential as an electrode material for lithium-ion batteries.[5] Since 2012, NVP has been studied as the electrode material for sodium-ion batteries.[6] NVP can act either as a positive or negative electrode material, with three distinguished compositions: $NaV_2P_3O_{12}$ – $Na_3V_2P_3O_{12}$ – $Na_4V_2P_3O_{12}$.[6a,7] During desodiation, vanadium(III) is oxidized to V(IV) at the potential of about 3.4 V vs. Na^+/Na, giving a specific capacity of about 120 mAh g^{-1}; in the sodiation reaction, V(III) is reduced to V(II/III) at about 1.7 V with about 60 mAh g^{-1}.[6a] NVP also shows very promising capability in all-solid-state sodium batteries (Na-ASSBs). Having the same structure as the highly conductive solid electrolyte $Na_{3.4}Zr_2Si_{2.4}P_{0.6}O_{12}$ (NZSP),[8] NVP showed excellent compatibility with this electrolyte when used as the positive electrode material.[9]

NVP is supposed to have limited ionic and electronic conductivities, similar to another phosphate electrode material, $LiFePO_4$.[10] Various methods have been used to enhance its conductivities, including the use of *nano*-sized particles[11] and carbon coatings.[11a,12] However, the electrochemical behavior of NVP has rarely been studied systematically: its conductivity was just described as "low" in most papers.[6a,b,11b,12b,f,i,13] Wang et al. prepared densified sheets of NVP mixed with $60Na_2O$-$10Nb_2O_5$-$30P_2O_5$ glass and measured the conductivities of the mixtures (2.9×10^{-5} S cm^{-1} at room temperature).[14] Chekannikov et al. measured the impedance of carbon-coated NVP,[13r] and Li et al. carried out a direct current measurement on carbon-coated NVP.[13v] Pure and dense NVP samples are difficult to prepare, with V(III) and P(V) obtained at the same time during the sintering. Measurements in NIBs with liquid electrolyte, where NVP particles are surrounded by liquid electrolyte, can only indicate the overall performance of the powder sample, without any geometric information for further analysis of the material. It is also important to study the potential dependency of NVP's conductivity, since NVP is mainly used as an electrode material with changing potential during battery operation. In our previous work,[9,15] we noted the rapidly increasing polarization of Na-ASSB cells during high-rate charge/discharge, which is possibly related to the conducting behavior of NVP.

Here electrochemical cells were prepared with a tri-layered structure: a thin layer of NVP and Na foil as the cathode and anode, respectively, with an NZSP pellet in between. In such cells, the geometric parameters of NVP are known and

[a] T. Lan, Dr. Q. Ma, Dr. C.-L. Tsai, Dr. F. Tietz, Prof. O. Guillon
Forschungszentrum Jülich GmbH,
Institute of Energy and Climate Research
Materials Synthesis and Processing (IEK-1)
52425 Jülich, Germany
E-mail: t.lan@fz-juelich.de
[b] T. Lan, Prof. O. Guillon
Institute of Mineral Engineering
RWTH Aachen University
52062 Aachen, Germany
[c] T. Lan, Prof. O. Guillon
Jülich Aachen Research Alliance,
JARA-Energy
52425 Jülich, Germany
[d] Dr. C.-L. Tsai
Current address:
Forschungszentrum Jülich GmbH,
Institute of Energy and Climate Research
Fundamental Electrochemistry (IEK-9)
52425 Jülich, Germany

Supporting information for this article is available on the WWW under https://doi.org/10.1002/batt.202000229

Special Collection An invited contribution to a joint Special Collection between ChemElectroChem and Batteries & Supercaps dedicated to research Beyond Lithium-Ion Batteries

© 2020 The Authors. Batteries & Supercaps published by Wiley-VCH GmbH. This is an open access article under the terms of the Creative Commons Attribution License, which permits use, distribution and reproduction in any medium, provided the original work is properly cited.

© 2020 The Authors. Batteries & Supercaps published by Wiley-VCH GmbH

quantifiable, and the potential of NVP (vs. Na^+/Na) equals the voltage of the cell. The impedance spectra of these NVP|NZSP|Na cells were analyzed at various potentials and confirmed the process of Na migration into and out of NVP, thus NVP's ionic conductivity was calculated in dependence of the potential. Further analysis of the influence of NVP's conductivity on the performance of all solid-state sodium batteries (Na-ASSBs) was performed.

2. Results and Discussion

The cell design of this work is shown in Figure 1. In this tri-layered structure, the electrochemical potential can be controlled by adjusting the voltage of the cell. During potentiostatic electrochemical impedance spectroscopy (PEIS) measurement, most of the possible processes are in series connection, which simplifies the process of analysing of the data. As shown in Figure 1a, after heat-treatment, a dense layer of NVP formed on the surface of the NZSP pellet. The average thickness of the NVP layer was 1.7 μm, as calculated from 10 different scanning electron microscopy (SEM) images.

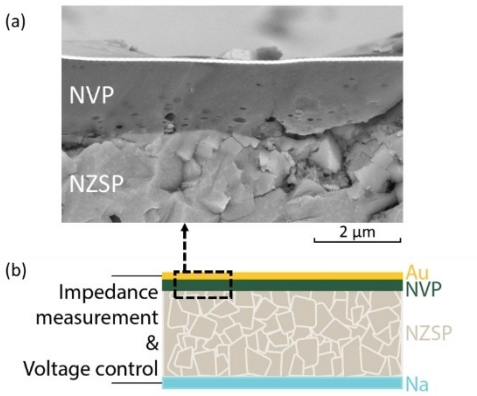


Figure 1. a) SEM image of NVP|NZSP|Na cell, obtained at the cross-section near the NVP|NZSP interface; b) sketch of the structure of the cell.

PEIS of the NVP|NZSP|Na cell was measured at various voltages at 25 °C. The impedance spectra of this cell structure can be interpreted by taking advantage of the impedance responses of NZSP and Na|NZSP|Na cells reported previously.[9,16] Since the Na negative electrode did not change during the measurement, the voltage of the cell equaled that of the potential of NVP (vs. Na^+/Na). PEIS was measured at voltages with smaller steps around 3.4 V, where the electrode reaction $Na_3V_2P_3O_{12} \rightarrow NaV_2P_3O_{12}$ happens (Figure S1 in supporting information). The PEIS of the NVP|NZSP|Na cell has two semicircles visible in each Nyquist plot, as shown in Figure 2a. The first and smaller one occurs at exactly the same frequencies (>1 MHz) and has comparable diameters (100–200 Ω) with that of NZSP grain boundary resistance reported previously.[16] The second semicircle at low frequencies, changing with cell voltages, or the potentials of NVP, is attributed to a process in the electrode material. The change of the second semicircle can be resolved in 3 stages: in Stage I (2.9–3.375 V), the diameter of the second semicircle increases only slightly; in Stage II (3.4–3.45 V), the diameter increases more compared to that in Stage I; a dramatic increase in diameter happens in Stage III (3.5–3.7 V). These changes indicate the relation between the second semicircle and the compositional change of NVP with increasing potential: the concentration of Na^+ in $Na_3V_2P_3O_{12}$ decreases with increasing potential from 2.9 V to

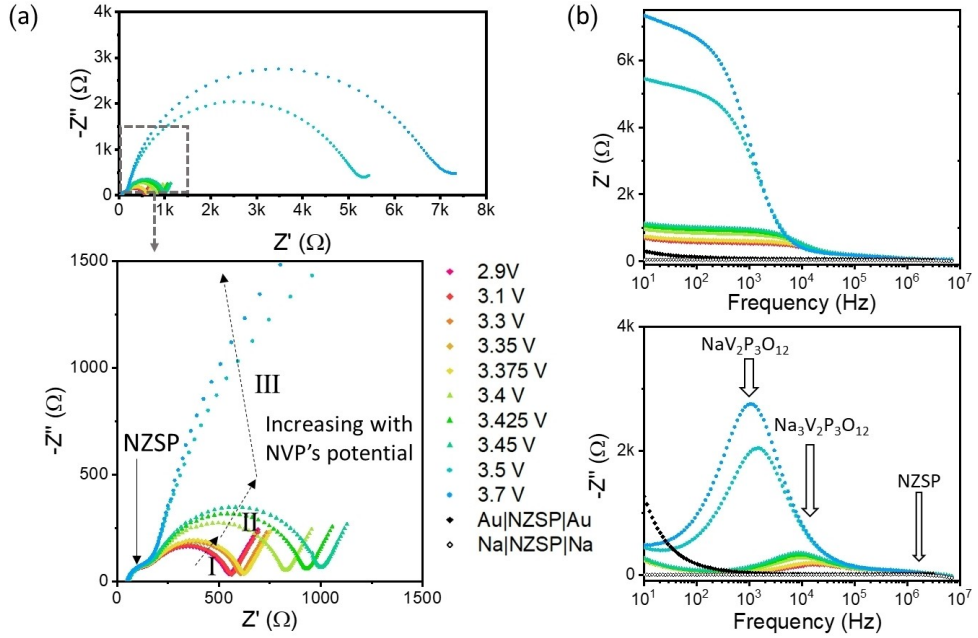


Figure 2. a) Nyquist plots of the PEIS results (7 MHz–10 Hz) measured on an NVP|NZSP|Na cell at various voltages, with the figure below showing more details near the coordinate origin; b) real (above) and imaginary (below) parts of the PEIS results of the NVP|NZSP|Na cell. Plots of a cell with blocking electrodes, Au|NZSP|Au, and non-blocking electrodes, Na|NZSP|Na, are shown for comparison.

© 2020 The Authors. Batteries & Supercaps published by Wiley-VCH GmbH

3.4 V. The $Na_3V_2P_3O_{12} \rightarrow Na_{1+x}V_2P_3O_{12}$ reaction takes place at ~3.4 V. At higher potentials, $Na_{1+x}V_2P_3O_{12}$ fully desodiates to $NaV_2P_3O_{12}$, a phase with smaller lattice parameters.[9]

Real and imaginary parts of the PEIS results at various potentials are shown in Figure 2b, together with reference plots of an Au|NZSP|Au cell and an Na|NZSP|Na cell (data from previous work).[15,16] At low frequencies (< 10 kHz), the Au|NZSP|Au cell shows a process of increasing impedance, more in the imaginary part and less in the real part, assigned to the ion-blocking effect of the Au electrode. The NVP|NZSP|Na cell, with a similar Au current collector on the positive electrode, also shows a similar process. The Na electrode is usually undetectable and the Na|NZSP interface usually appears at very low frequencies (~1 Hz).[15] At about 10 kHz, NVP|NZSP|Na shows one obvious process that does not exist in symmetric cells. The real part of the impedance is constantly higher than that of symmetric cells while the imaginary part of this process shows an increasing peak. For $Na_3V_2P_3O_{12}$ (< 3.5 V) the peak width ranges from 1 kHz to 100 kHz. During the desodiation of NVP, the impedance increases slightly, probably due to a lower amount of Na^+ ions in the lattice. Beyond a critical Na^+ concentration (between 3.45 and 3.5 V) a phase transition occurs leading to an abrupt decrease of the unit cell volume,[9] combined with a dramatic change of the electrochemical process resulting in a shift of the response frequency to about 1 kHz and a strong increase in impedance. However, it is still unclear if the NVP|NZSP interface influences the impedance of the cell.

In order to further interpret the electrochemical behavior of NVP, distributions of relaxation times (DRT) are calculated from the PEIS results shown in Figure 2. DRT is a model that separates time-dependent polarization processes, obtained from Equation (1):

$$Z(f) = R_\infty + \int_0^\infty \frac{\gamma(ln\tau)}{1 + i2\pi f\tau} dln\tau \quad (1)$$

where R_∞ is the ohmic resistance, f is the frequency, and $\gamma(ln\tau)$ is a fitting function that describes the time (τ)-dependent polarization processes.[17] As summarized in Figure 3a, the DRT peaks can be divided into four regions. The first region ($\tau < 10^{-6}$ s) is similar to NZSP cells without an NVP electrode,[15,16] and remains unchanged with the cell voltage. Thus, this region can be assigned to the grain boundary conductivity of NZSP. The last region ($\tau > 0.02$ s) contains peaks related to the ion-blocking effects from the Au current collector, as the "tails" shown in Figure 2(a). The second and third regions contain peaks changing with the cell voltage and are related to NVP. In the second region, there are four overlapping peaks, namely **P1**–**P4**. In order to have a clear visualization of these peaks, the highest γ of each voltage is normalized in Figure 3b. As shown in Figure 2a and b, the response time of the dominant peak of NVP changes with increasing potential: in Stage I, the dominant peak is **P1**; **P1** decreases with increasing potential, while **P2** increases and becomes the dominant peak in Stage II; in Stage III, after the phase transformation, **P3** becomes dominant and **P4** also increases. The switch of dominance of peaks in the second region is probably related to the two different ways of Na^+ migration in NaSICON-structured materials. There are two different Na^+ sites in the NaSICON structure, namely A(1) and A(2); in NVP, Na ions in A(1) sites tend to remain immobile.[5,18] After the phase change (Stage III), however, NVP loses most of its Na^+ in A(2) sites, and thus the Na^+ migration mode changes. Similar change caused by phase transformation was also observed in the Na^+ migration driven by the magnetic field.[19] The third region contains two peaks increasing and shifting towards smaller τ values with higher potential. It is still impossible to have an unambiguous assignment of these peaks to the NVP-NZSP interface or NVP phase. These processes have a smaller resistance but a much higher τ value. Thus, the capacitance is much higher and probably related to the interface between NVP and NZSP.[20] Similar shift cannot be found in **P4**, which is then assigned to the NVP phase. Also, peaks in the third region contribute much less to the total impedance than peaks in the second region, so these assignments do not influence the order of magnitude of the total resistance. Based on these assumptions, the calculation of the conductivity of NVP is based on the frequency range of the second region.

A model with paralleled resistance and constant phase element (CPE) is used to fit the semicircles in this range and the results are listed in Table 1. The CPE is a non-intuitive circuit

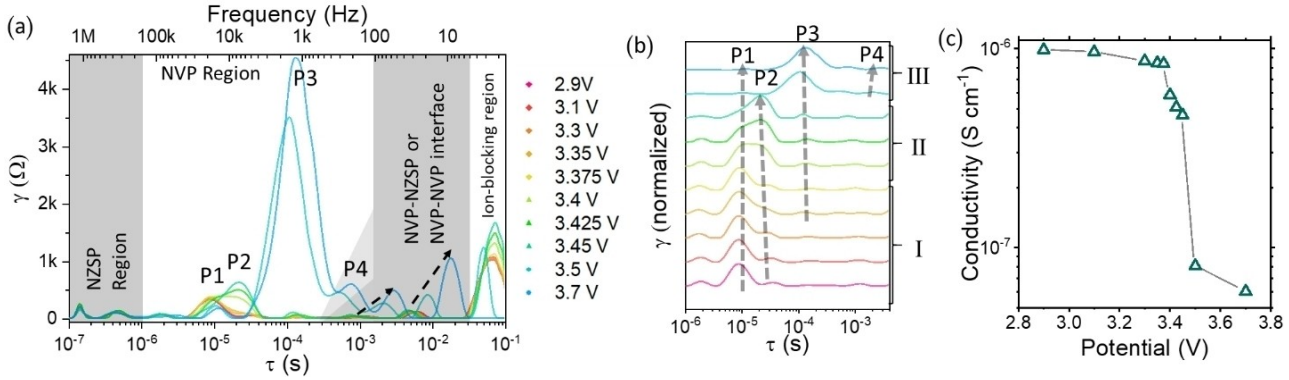


Figure 3. a) DRT of an NVP|NZSP|Na cell at different voltages; b) central part of the DRT results with normalized γ; c) estimated conductivity of NVP depending on applied potential.

© 2020 The Authors. Batteries & Supercaps published by Wiley-VCH GmbH

Table 1. Fitting results of PEIS data in Figure 2b, based on the frequency ranges of NVP phase obtained in Figure 3a.

Potential [V]	Resistance [Ω]	CPE [F]	n of CPE
2.9	4.1×10^{2}	1.2×10^{-7}	0.85
3.1	4.2×10^{2}	1.2×10^{-7}	0.85
3.3	4.6×10^{2}	1.2×10^{-7}	0.85
3.35	4.7×10^{2}	1.1×10^{-7}	0.86
3.375	4.8×10^{2}	1.1×10^{-7}	0.85
3.4	6.9×10^{2}	1.1×10^{-7}	0.85
3.425	7.9×10^{2}	1.1×10^{-7}	0.85
3.45	8.7×10^{2}	1.1×10^{-7}	0.85
3.5	4.9×10^{3}	6.7×10^{-8}	0.88
3.7	6.7×10^{3}	6.2×10^{-8}	0.89

element used to describe imperfect capacitance. The impedance of a CPE is defined as $Z_{CPE} = CPE^{-1} \times (i\omega)^{-n}$, where n is the constant phase, ranging normally between 0.5 and 1 with $n=1$ for a perfect capacitance. As shown in Table 1, the resistance of NVP increases with increasing potential, which will be discussed in detail later. Meanwhile, the CPE decreases slightly from 1.2×10^{-7} F to 0.6×10^{-7} F. Considering the geometric morphology of the NVP layer (~1.7 μm thick, Figure 1), the capacitance of the material is similar to that of other NaSICON materials, since the capacitance of an element is inversely proportional to its thickness.[16] The constant phase n stays constant at 0.85 below 3.45 V and increases to 0.89 with 3.5 and 3.7 V. It is still unknown if the change of CPE is related to the changing of Na^+ migration mode in NVP.

Figure 3c summarizes the conductivities of NVP at various potentials, calculated from the resistance in Table 1 and the geometric factors of the NVP layer ($\sigma = h \times A^{-1} \times R^{-1}$, where h, A, and R are the average thickness, total area, and resistance of NVP, respectively). From 2.9 V to 3.375 V (Stage I), the conductivity decreased slightly in the range of 10^{-6} S cm^{-1}, probably due to the extraction of Na^+. In this stage, concerted ion migration takes place due to the high number of charge carriers and the low number of vacancies. During the $Na_3V_2P_3O_{12} \rightarrow NaV_2P_3O_{12}$ reaction (Stage II), the conductivity of the material decreased by an order of magnitude with increasing potential, with more single ion jumps due to the increased number of vacancies. After further desodiation (Stage III), the $NaV_2P_3O_{12}$ phase showed a much lower conductivity than that of $Na_{1+x}V_2P_3O_{12}$. As discussed before, in this stage, strongly bonded Na^+ at an A(1) site resists being replaced by jumps of A(2) ions. This change is also related to the lattice shrinkage of the material, which agrees well with the correlation between crystal structures and conductivities reported in other NaSICON materials.[21] At all potentials, the ionic conductivity of NVP is much lower than that of NZSP, typically $1–5\times10^{-3}$ S cm^{-1}.[22]

The electrochemical behavior of NVP influences the performance of Na-ASSB cells. Na-ASSB cells prepared by chemical infiltration were able to be charged and discharged at 0.5 C and those with small loadings at 1 C.[9,15] This C-rate is a breakthrough for ASSBs, achieved by low internal resistance of the cells. However, 1 C is still not enough for practical application in many cases. In contrast, NVP in batteries with liquid electrolyte were able to operate at much higher C-rates (up to 10 C).[12a] Compared to batteries with liquid electrolyte, Na-ASSB cells showed much higher polarization during cycling.[12a,13o] Figure 4a shows typical charge/discharge curves of ASSB cells, obtained from a C-rate test of an NVP | NZSP | Na cell, prepared by a chemical infiltration method we reported previously.[9,15] For a better comparison of polarization, a shifted capacity, $C - 0.5\ C_{max}$, is chosen as the x-axis, where the capacity C is shifted by half of C_{max}, the maximum capacity of the respective charge/discharge half cycle. When operated at higher C-rate, higher polarization can be observed: the voltage gap between the charge and discharge curves became larger; both curves also show steeper slopes. More details of the C-rate tests can be found in Figure S2 in the supporting information. Similar phenomenon can also be observed in batteries with $LiFePO_4$ as the positive electrode material, as shown in Figure 4b with data taken from a previous report.[23] Na-ASSB cells prepared by chemical infiltration have similar internal resistance as cells with liquid electrolyte.[9,12a] Thus, there must exist other factors that prevent the ASSB cells from fast charging/discharging.

Figure 4c shows a sketch of a typical charge/discharge curve of NVP | NZSP | Na cells, in which the x-axis represents the Na^+ amount in NVP. It is clear that the deviation of the discharge curve from the equilibrium cannot be explained by ohmic polarization, whose contribution will result in plateaus paralleled to the 3.4 V equilibrium line in the case of constant ohmic resistance. The internal resistance should increase with less Na^+ in NVP, as shown by the dash lines in Figure 4d, while in the discharge curve of a real cell, as shown in Figure 4c, the slope is inverse. The deviation of potential, then, is only related to operation time and can be explained by the concentration polarization inside the less conductive NVP phase. This assumption can be further confirmed by variation of the current and how the curves change with higher operation current, as shown in Figure 4e. The deviation of the discharge curve from the equilibrium state increases with increasing current. Concentration polarization, as the C-rate limiting factor, can also explain the difference between an ASSB cell and a cell with a liquid electrolyte. In the latter case the NVP particles have a much smaller average size (several hundred nm) and are surrounded by liquid electrolyte;[6b,13o,r,24] while in an ASSB prepared by chemical infiltration, only electrode material is in contact with the solid electrolyte on one side of the particle/film. In order to enable ASSB cells with higher C-rate, it is necessary to further reduce the particle size of active electrode material. Thus, the pathway of ion transport in the less conductive electrode material is shorter, and the concentration polarization can be reduced.

3. Conclusions

In summary, the electrochemical behavior of NVP was characterized in an ASSB cell with impedance methods. The ionic conductivity of NVP was measured for the first time with controlled geometric factors. At 25 °C, NVP showed a total conductivity of 1×10^{-6} S cm^{-1} at 2.9 V, and the conductivity

© 2020 The Authors. Batteries & Supercaps published by Wiley-VCH GmbH

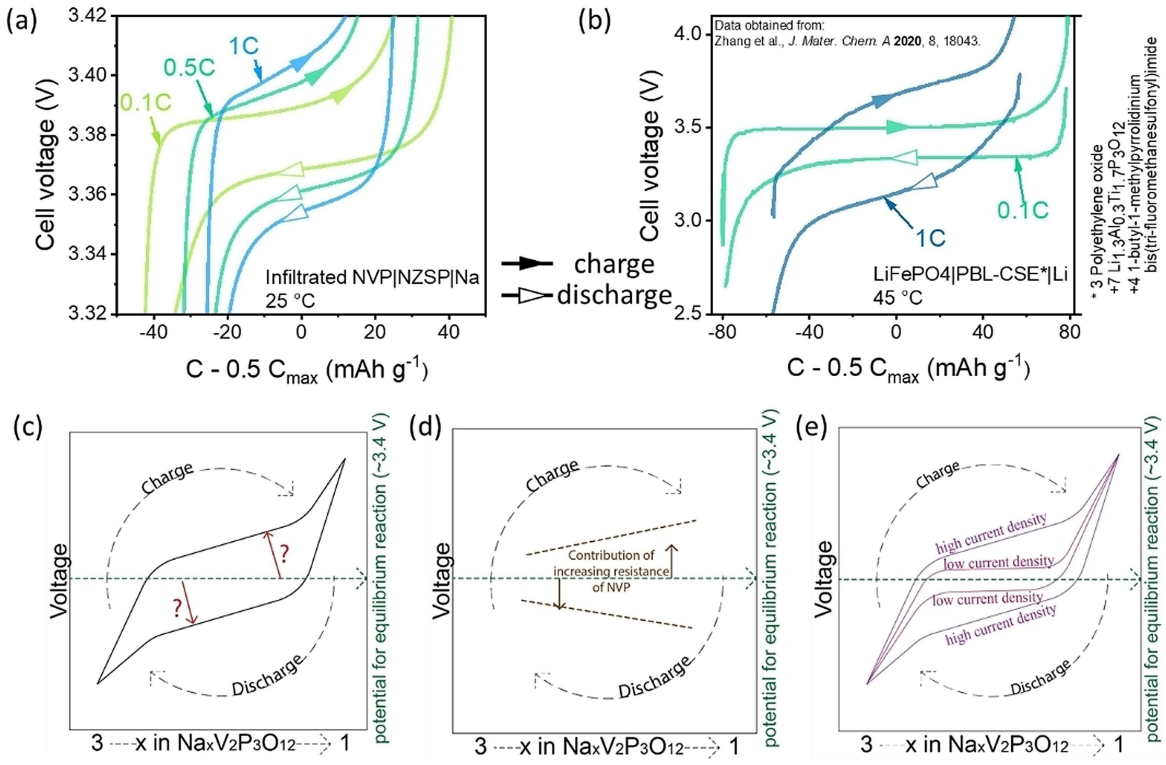


Figure 4. a) The charge/discharge curves of an infiltrated NVP | NZSP | Na ASSB cell operating at different C-rates (here *n* C means the cell is fully charged/discharged in 1/*n* hours, a shifted capacity ($C - 0.5C_{max}$, see text for more information) is chosen as x-axis for a better comparison of polarization; b) the charge/discharge curves of a polymer-based battery cell using $LiFePO_4$ as the positive electrode material, data obtained from Zhang et al.;[23] c) the typical shape of charge/discharge curves of an NVP | NZSP | Na ASSB cell, with Na concentration as the x-axis; d) contribution of ohmic resistance to the charge/discharge curve of an ASSB cell; e) The influence of increasing current on charge/discharge curve of a typical NVP | NZSP | Na ASSB cell.

decreased with higher potential of NVP to 8×10^{-8} S cm^{-1} at 3.5 V, mainly due to the strong bonding of Na^+ at A(1) sites in the NVP lattice This low conductivity, especially at higher voltages, influences the performance of Na-ASSBs with an NVP electrode, especially the high-rate performance. Small particle sizes of NVP are required in electrode composites, in order to reduce the ohmic polarization and concentration polarization. This optimization is the key to increasing the power density of Na-ASSBs with electrodes using NVP or similar materials.

Experimental Section

Na-ASSBs with thin layer NVP electrodes were prepared by dropping an NVP precursor solution onto sintered NZSP pellets followed by heat-treatment. The NVP precursor solution was made by mixing ethanolamine (Merck, boiling point: 170 °C), deionized H_2O, NaH_2PO_4 (Sigma-Aldrich), and NH_4VO_3 (Merck) (weight ratio 1:2:0.71:0.46). NZSP powder was synthesized by a solution-assisted solid-state reaction[16,25] dissolving $NaNO_3$ (VWR), $ZrO(NO_3)_2$ (Aldrich), $Si(OCH_2CH_3)_4$ (Merck), and $NH_4H_2PO_4$ (Merck) in deionized H_2O. The mixture was dried at 85 °C and then calcined at 800 °C. The calcined powder was milled in ethanol with zirconia balls on a milling bench for 48 h. NZSP powder was put into a cylindrical pressing mold (diameter 13 mm), and then pressed into pellets using an uniaxial press with a pressure of 90 MPa. The pressed pellets were sintered in air at 1280 °C for 6 h. One drop of the precursor solution was deposited onto the surface. The pellets were then heated to 740 °C in Ar-2% H_2 for 4 h to form the NVP phase. Au was sputtered on the NVP layer to serve as a current collector. Sodium (Sigma-Aldrich) was attached to the opposite surface of the NZSP pellet in an Ar-filled glovebox. The cells were sealed in Swagelok shells after assembling.

Na-ASSBs with chemically infiltrated NVP were prepared by infiltrating NVP precursor solution into the porous layer of sintered porous-dense bi-layered NZSP pellets followed by heat-treatment. To produce the dense-porous bi-layered NZSP pellets, NZSP powder was mixed with 10 wt.% rice starch (BENEO-Remy) by ball-milling in ethanol for 24 h. 0.3–0.4 g NZSP powder and 20 mg of the mixture were subsequently put into a cylindrical pressing mold (diameter 13 mm) layer by layer, and pressed into pellets using a uniaxial press with a pressure of 90 MPa. The pressed pellets were sintered in air at 1280 °C for 6 h. The NVP precursor solution was made by ethanolamine (Merck, boiling point: 170 °C), deionized H_2O, NaH_2PO_4 (Sigma-Aldrich), NH_4VO_3 (Merck), and citric acid (Merck) (weight ratio 1:2:0.71:0.46:1). Drop of the solution was deposited onto the surface of the porous layer for infiltration and propagated by capillary force. The pellets were then heated to 740 °C in Ar-2% H_2 for 4 h to form the NVP phase. The infiltration and heating process was repeated 3 times to obtain the desired loading of active material and establish continuous electronic pathways. Au was sputtered on the NVP layer to serve as a current collector. Sodium (Sigma-Aldrich) was attached to the opposite surface of the NZSP pellet in an Ar-filled glovebox. The cells were sealed in Swagelok shells after assembling.

Electrochemical measurements were performed with a multi-channel potentiostat (Biologic VMP-300) at a constant temperature of 25 °C in a climate chamber (Vötsch, VT4002). Potentiostatic

© 2020 The Authors. Batteries & Supercaps published by Wiley-VCH GmbH

electrochemical impedance spectroscopy (PEIS) was carried out on cells at various voltages. The voltage was controlled using galvanostatic cycling with potential limitation (GCPL) followed by holding the battery cell at a given potential for at least 12 hours to ensure steady-state conditions. Data from the electrochemical measurements were processed using the programs EC-Lab, Z-view, and DRTtools[17a] (Gaussian discretization, $\lambda = 10^{-5}$, run in Matlab). Cyclic voltammetry (CV) tests were operated with a scanning rate of 0.5 mV s^{-1}. C-rate tests of the Na-ASSBs with chemically infiltrated NVP were performed between 0.1 and 1 C, cf. Figure S2.

Microstructures of cells were investigated by SEM (Zeiss Ultra55). Chemical analysis of cell components was performed by inductively coupled plasma optical emission spectrometry (ICP-OES, Thermo Scientific iCAP7600). The geometric factors of the NVP layer was calculated from the average thickness of the layer and the total weight of NVP.

Acknowledgements

The authors thank Dr. D. Sebold for SEM analysis, and Dr. V. Nischwitz for ICP-OES analysis. Partial financial support from China Scholarship Council (CSC) (file no. 201606210131) is gratefully acknowledged. Open access funding enabled and organized by Projekt DEAL.

Conflict of Interest

The authors declare no conflict of interest.

Keywords: sodium battery · all-solid-state battery · NaSICON · sodium vanadium phosphate · electrochemical impedance spectroscopy

[1] a) B. Dunn, H. Kamath, J.-M. Tarascon, *Science* **2011**, *334*, 928; b) D. Larcher, J.-M. Tarascon, *Nat. Chem.* **2015**, *7*, 19; c) N. Yabuuchi, K. Kubota, M. Dahbi, S. Komaba, *Chem. Rev.* **2014**, *114*, 11636; d) V. Palomares, P. Serras, I. Villaluenga, K. B. Hueso, J. Carretero-González, T. Rojo, *Energy Environ. Sci.* **2012**, *5*, 5884.

[2] a) H.-P. Hong, *Mater. Res. Bull.* **1976**, *11*, 173; b) M. E. Brownfield, E. E. Foord, S. J. Sutley, T. Botinelly, *Am. Mineral.* **1993**, *78*, 653; c) K. Chayambuka, G. Mulder, D. L. Danilov, P. H. L. Notten, *Adv. Energy Mater.* **2018**, *8*, 1800079.

[3] a) C. Delmas, R. Olazcuaga, F. Cherkaoui, R. Brochu, G. Le Flem, *C. R. Hebd. Seances Acad. Sci.* **1978**, *287*, 169; b) J. B. Goodenough, H. Y. P. Hong, J. A. Kafalas, *Mater. Res. Bull.* **1976**, *11*, 203.

[4] a) J. Gopalakrishnan, K. K. Rangan, *Chem. Mater.* **1992**, *4*, 745; b) V. Korthuis, R. Hoffmann, J. Huang, A. Sleight, *Chem. Mater.* **1993**, *5*, 206; c) I. V. Zatovsky, *Acta Crystallogr. Sect. E* **2010**, *66*, i12; d) Z. Jian, C. Yuan, W. Han, X. Lu, L. Gu, X. Xi, Y.-S. Hu, H. Li, W. Chen, D. Chen, Y. Ikuhara, L. Chen, *Adv. Funct. Mater.* **2014**, *24*, 4265.

[5] B. L. Cushing, J. B. Goodenough, *J. Solid State Chem.* **2001**, *162*, 176.

[6] a) Z. Jian, L. Zhao, H. Pan, Y.-S. Hu, H. Li, W. Chen, L. Chen, *Electrochem. Commun.* **2012**, *14*, 86; b) J. Kang, S. Baek, V. Mathew, J. Gim, J. Song, H. Park, E. Chae, A. K. Rai, J. Kim, *J. Mater. Chem.* **2012**, *22*, 20857; c) S. Chen, C. Wu, L. Shen, C. Zhu, Y. Huang, K. Xi, J. Maier, Y. Yu, *Adv. Mater.* **2017**.

[7] S. Y. Lim, H. Kim, R. Shakoor, Y. Jung, J. W. Choi, *J. Electrochem. Soc.* **2012**, *159*, A1393.

[8] a) Q. Ma, M. Guin, S. Naqash, C.-L. Tsai, F. Tietz, O. Guillon, *Chem. Mater.* **2016**, *28*, 4821; b) Q. Ma, F. Tietz, A. Leonide, E. Ivers-Tiffée, *Electrochem. Commun.* **2010**, *12*, 1326.

[9] T. Lan, C.-L. Tsai, F. Tietz, X.-K. Wei, M. Heggen, R. E. Dunin-Borkowski, R. Wang, Y. Xiao, Q. Ma, O. Guillon, *Nano Energy* **2019**, *65*, 104040.

[10] W.-J. Zhang, *J. Power Sources* **2011**, *196*, 2962.

[11] a) S. Li, Y. Dong, L. Xu, X. Xu, L. He, L. Mai, *Adv. Mater.* **2014**, *26*, 3545; b) S. Kajiyama, J. Kikkawa, J. Hoshino, M. Okubo, E. Hosono, *Chem. Eur. J.* **2014**, *20*, 12636.

[12] a) C. Zhu, K. Song, P. A. van Aken, J. Maier, Y. Yu, *Nano Lett.* **2014**, *14*, 2175; b) D. Zhou, R. Liu, J. Zhang, X. Qi, Y.-B. He, B. Li, Q.-H. Yang, Y.-S. Hu, F. Kang, *Nano Energy* **2017**, *33*, 45; c) W.-J. Wang, H.-B. Zhao, A.-B. Yuan, J.-H. Fang, J.-Q. Xu, *Acta Phys. Chim. Sinica* **2014**, *30*, 1113; d) J. Yan, X. Liu, B. Li, *Electrochem. Commun.* **2015**, *56*, 46; e) Y. Fang, L. Xiao, X. Ai, Y. Cao, H. Yang, *Adv. Mater.* **2015**, *27*, 5895; f) J. Liu, K. Tang, K. Song, P. A. van Aken, Y. Yu, J. Maier, *Nanoscale* **2014**, *6*, 5081; g) X. Rui, W. Sun, C. Wu, Y. Yu, Q. Yan, *Adv. Mater.* **2015**, *27*, 6670; h) W. Zhang, Y. Liu, C. Chen, Z. Li, Y. Huang, X. Hu, *Small* **2015**, *11*, 3822; i) H. Zhang, I. Hasa, B. Qin, T. Diemant, D. Buchholz, R. J. Behm, S. Passerini, *ChemElectroChem* **2017**, *4*, 1256.

[13] a) A. K. Padhi, K. Nanjundaswamy, J. B. Goodenough, *J. Electrochem. Soc.* **1997**, *144*, 1188; b) L. S. Plashnitsa, E. Kobayashi, Y. Noguchi, S. Okada, J.-i. Yamaki, *J. Electrochem. Soc.* **2010**, *157*, A536; c) Y. H. Jung, C. H. Lim, D. K. Kim, *J. Mater. Chem. A* **2013**, *1*, 11350; d) W. Shen, C. Wang, H. Liu, W. Yang, *Chem. Eur. J.* **2013**, *19*, 14712; e) W. Song, X. Ji, Y. Yao, H. Zhu, Q. Chen, Q. Sun, C. E. Banks, *Phys. Chem. Chem. Phys.* **2014**, *16*, 3055; f) Z. Chu, C. Yue, *Solid State Ionics* **2016**, *287*, 36; g) Z. Chu, C. Yue, *Ceram. Int.* **2016**, *42*, 820; h) J. Fang, S. Wang, Z. Li, H. Chen, L. Xia, L. Ding, H. Wang, *J. Mater. Chem. A* **2016**, *4*, 1180; i) Q. Hu, J.-Y. Liao, B.-K. Zou, H.-Y. Wang, C.-H. Chen, *J. Mater. Chem. A* **2016**, *4*, 16801; j) R. Klee, P. Lavela, M. J. Aragon, R. Alcantara, J. L. Tirado, *J. Power Sources* **2016**, *313*, 73; k) R. Rajagopalan, L. Zhang, S. X. Dou, H. K. Liu, *Adv. Mater. Interfaces* **2016**, *3*; l) W. Shen, H. Li, Z. Guo, C. Wang, Z. Li, Q. Xu, H. Liu, Y. Wang, Y. Xia, *ACS Appl. Mater. Interfaces* **2016**, *8*, 15341; m) J. Song, S. Park, V. Mathew, J. Gim, S. Kim, J. Jo, S. Kim, M. H. Alfaruqi, J. P. Baboo, I. H. Kim, S. J. Song, J. Kim, *ACS Appl. Mater. Interfaces* **2016**, *8*, 35235; n) S. Tao, P. Cui, W. Huang, Z. Yu, X. Wang, S. Wei, D. Liu, L. Song, W. Chu, *Carbon* **2016**, *96*, 1028; o) Y. Xu, Q. Wei, C. Xu, Q. Li, Q. An, P. Zhang, J. Sheng, L. Zhou, L. Mai, *Adv. Energy Mater.* **2016**, *6*; p) X. Zhong, Z. Yang, Y. Jiang, W. Li, L. Gu, Y. Yu, *ACS Appl. Mater. Interfaces* **2016**, *8*, 32360; q) C. Zhu, P. Kopold, P. A. van Aken, J. Maier, Y. Yu, *Adv. Mater.* **2016**, *28*, 2409; r) A. Chekannikov, R. Kapaev, S. Novikova, N. Tabachkova, T. Kulova, A. Skundin, A. Yaroslavtsev, *J. Solid State Electrochem.* **2017**, *21*, 1; s) R. Klee, M. Wiatrowski, M. J. Aragon, P. Lavela, G. F. Ortiz, R. Alcantara, J. L. Tirado, *ACS Appl. Mater. Interfaces* **2017**, *9*, 1471; t) C. Delmas, A. Nadiri, J. L. Soubeyroux, *Solid State Ionics* **1988**, *28*, 419; u) H. Huang, S. C. Yin, T. Kerr, N. Taylor, L. F. Nazar, *Adv. Mater.* **2002**, *14*, 1525; v) H. Li, X. Yu, Y. Bai, F. Wu, C. Wu, L.-Y. Liu, X.-Q. Yang, *J. Mater. Chem. A* **2015**, *3*, 9578.

[14] H. Wang, G. Hasegawa, Y. Akiyama, T. Yamamoto, A. Inoishi, H. Akamatsu, M. Inada, T. Ishihara, K. Hayashi, *Electrochim. Acta* **2019**, *305*, 197.

[15] C.-L. Tsai, T. Lan, C. Dellen, Y. Ling, Q. Ma, D. Fattakhova-Rohlfing, O. Guillon, F. Tietz, *J. Power Sources* **2020**, *476*, 228666.

[16] Q. Ma, C. Tsai, X. K. Wei, M. Heggen, F. Tietz, J. T. S. Irvine, *J. Mater. Chem. A* **2019**, *7*, 7766.

[17] a) T. H. Wan, M. Saccoccio, C. Chen, F. Ciucci, *Electrochim. Acta* **2015**, *184*, 483; b) V. Sonn, A. Leonide, E. Ivers-Tiffée, *J. Electrochem. Soc.* **2008**, *155*, B675.

[18] W. Song, X. Ji, Z. Wu, Y. Zhu, Y. Yang, J. Chen, M. Jing, F. Li, C. E. Banks, *J. Mater. Chem. A* **2014**, *2*, 5358.

[19] Z. Jian, *Ph.D. theis*, Wuhan University of Technology, Wuhan **2012**.

[20] J. T. Irvine, D. C. Sinclair, A. R. West, *Adv. Mater.* **1990**, *2*, 132.

[21] M. Guin, F. Tietz, O. Guillon, *Solid State Ionics* **2016**, *293*, 18.

[22] Q. Ma, F. Tietz, *ChemElectroChem* **2020**, *7*, 2693.

[23] D. Zhang, X. Xu, X. Huang, Z. Shi, Z. Wang, Z. Liu, R. Hu, J. Liu, M. Zhu, *J. Mater. Chem. A* **2020**, *8*, 18043.

[24] J. Zhang, Y. Fang, L. Xiao, J. Qian, Y. Cao, X. Ai, H. Yang, *ACS Appl. Mater. Interfaces* **2017**, *9*, 7177.

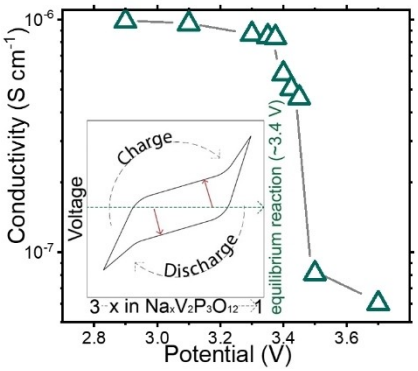
[25] S. Naqash, Q. Ma, F. Tietz, O. Guillon, *Solid State Ionics* **2017**, *302*, 83.

Manuscript received: October 1, 2020
Revised manuscript received: October 23, 2020
Accepted manuscript online: November 10, 2020
Version of record online: ■■, ■■■

© 2020 The Authors. Batteries & Supercaps published by Wiley-VCH GmbH

ARTICLES

Conductivity matters: The ionic conductivity of $Na_3V_2P_3O_{12}$ (NVP) was measured in an all-solid-state battery cell with thin layer NVP electrode deposited from precursor solution. It decreases with increasing electrochemical potential from 1×10^{-6} S cm^{-1} at 2.9 V to 8×10^{-8} S cm^{-1} at 3.5 V. This low conductivity acts as the key limitation to the high-rate cycling of all-solid-state batteries.



T. Lan, Dr. Q. Ma, Dr. C.-L. Tsai, Dr. F. Tietz, Prof. O. Guillon*

1 – 7

Ionic Conductivity of $Na_3V_2P_3O_{12}$ as a Function of Electrochemical Potential and its Impact on Battery Performance